Inorganic Chemistry

Local Structure of Actinide Dioxide Solid Solutions $Th_{1-x}U_xO_2$ and $Th_{1-x}Pu_xO_2$

S. Hubert,[*,†] **J. Purans,**[†] **G. Heisbourg,**[†] **P. Moisy,**[‡] **and N. Dacheux**[†]

Institut de Physique Nucléaire, Université Paris Sud, 91406-Orsay, France, and CEA/Valrhô DRCP/SCPS, BP 17171, 30207 Bagnols/Cèze Cedex, France

Extended X-ray absorption fine structure (EXAFS) has been utilized to investigate the local atomic structure around Th, U, and Pu atoms in polycrystalline mixed dioxides $Th_{1-x}M_xO_2$ (with M = U, Pu) for *x* ranging from 0 to 1. The composition dependence of the two first-coordination-shell distances was measured throughout the entire composition range for both solid solutions. The first-shell distances vary slightly across the solid-solution composition with values close to those of the pure dioxide parents, indicating a bimodal cation−oxygen distribution. In contrast, the second-shell distance varies strongly with composition, with values close to the weighted amount average distances. Nevertheless, in both systems, the lattice cell parameters, deduced from the first- and second-shell bond determined by EXAFS, are very close to those measured from X-ray diffraction (XRD). They vary linearly with composition, accurately following Vegard's law.

Introduction

In the past decade, there has been a renewal of interest in studying the feasibility of thorium-based fuel reactors as a potential advanced fuel for Generation IV nuclear energy systems producing fewer minor actinides than in uranium-based fuel.[1,2] However, in such thorium-based fuel, mixed dioxides containing fissile and fertile materials are required for starting the nuclear reaction, such as ThO_2 containing $^{235}UO_2$ or $^{239}PuO_2$. Such future nuclear fuels (U- and Th-based fuels) are made of solid solution ThO_2−UO_2, ThO_2−PuO_2, or UO_2−PuO_2.

ThO_2, UO_2, and PuO_2 are isomorphic, with a face-centered cubic lattice (fcc) of the fluorite type structure, with similar lattice parameters: *a* = 5.5975, 5.4704, and 5.396 Å, respectively.[3−6] Consequently, the difference in ionic radii between Th^{4+} (1.05 Å) and U^{4+} (0.997 Å) is smaller than the difference between Th^{4+} and Pu^{4+} (0.962 Å).[7−9] The

ThO_2−UO_2 binary system was extensively studied by various investigators,[10,11] who showed that UO_2 and ThO_2 form a continuous series of fcc solid solutions. The lattice parameter was observed to decrease linearly with increasing uranium concentration, closely following Vegard's law over the entire composition range. However, Christensen[12] found a significant departure from ideal solid solubility. Cohen and Berman[4] reported that the lattice parameter for a U−Th mixed dioxide deviated from Vegard's law at around 2 at % thorium concentration, indicating the formation of some kind of short-range ordering or clustering. Beauvy[6] observed divergence from the classical Vegard's law[5] as well for the stoichiometric mixed dioxide UO_2−PuO_2 up to approximately 5 at % plutonium. However, above 5 at %, it was shown to obey Vegard's law. This behavior was not confirmed by Tsuji et al.[13]

In the case of ThO_2−PuO_2 mixed oxide, magnetic measurements made by Dawson[14] imply that a solid solution

---

* To whom correspondence should be addressed. Phone: 33-1-69157344. Fax: 33-1-69157150. E-mail: shubert@ipno.in2p3.fr.
† Université Paris Sud.
‡ CEA/VALRHO DRCP/SCPS.

(1) Herring, J. S.; MacDonald, P. E.; Weaver, K. D.; Kullberg, C. *Nucl. Eng. Des.* **2001**, *203*, 65−71.
(2) Fourest, B.; Vincent, T.; Lagarde, G.; Hubert, S.; Baudoin, P. *J. Nucl. Mater.* **2000**, *282*, 180−185.
(3) Zachariasen, W. H. *Phys. Rev.* **1948**, *73*, 1104−1105.
(4) Cohen, I.; Berman, R. M. *J. Nucl. Mat.* **1966**, *18*, 77−107.
(5) Mulford, R. N. R.; Ellinger, E. H. *J. Am. Ceram. Soc.* **1958**, *80*, 2023−2026.
(6) Beauvy, M. *J. Nucl. Mater.* **1992**, *188*, 232−238.

(7) Shannon, R. D. *Acta Crystallogr., Sect. A* **1976**, *32*, 751−767.
(8) David, F. *J. Less Common Met.* **1986**, *121*, 27−35.
(9) Katz, J.; Seaborg, G.; Morss, L. *The Chemistry of the Actinides Elements*; Chapman and Hall: London, 1986.
(10) Slowinski, E.; Elliot, N. *Acta Crystallogr.* **1952**, *5*, 768−770.
(11) Lambertson, W. A.; Mueller, H. H.; Gunzel, F. H. *J. Am. Ceram. Soc.* **1953**, *36*, 365−368.
(12) Christensen, J. A. Report HW-76559; Hanford Works: Richland, WA, 1963; p 115.
(13) Tsuji, T.; Iwatsushige, M.; Yamashita, T.; Ohuchi, K. *J. Alloys Compd.* **1998**, *271*, 391−394.

following Vegard's law exists. Only one paper reports on the investigation of an X-ray lattice parameter.[15] A linear variation of the lattice parameter with composition was observed that follows Vegard's law within the accuracy of the measurements.

Crystallographic structure and lattice parameters have been investigated as a function of the composition for the mixed-actinide dioxides ThO_2-UO_2, UO_2-PuO_2, and ThO_2-PuO_2 using X-ray diffraction techniques. However, crystallographic approaches provide essential information on the average structure but no information on the local structure of atoms in crystals. Vegard's law states that the lattice parameter of a solid solution is equal to the sum of the lattice parameters of individual components weighted by their associated concentration. In this model, considering the composition dependence of the two bond lengths in solid solutions, two limiting possibilities are recognized. Bond length can be considered either composition independent (Bragg–Pauling) or composition dependent with linear variation (Virtual Crystal Approximation (VCA)).[16,17] In the latter hypothesis, the atoms are located on ideal lattice sites of the average unit cell, and the sublattice assumes an average value of bond length, whereas in the former, bond length remains constant whatever the composition.

The local structure of such solid solutions has not yet been investigated using EXAFS. Only pure actinide dioxides ThO_2, UO_2, and PuO_2 have been extensively studied.[18–20] Nevertheless, one reports an EXAFS study on $(U, Ce)O_2$, showing that the variation of first- and second-neighbor distances with composition obeys Vegard's law without bimodal distribution between 0 and 50 at %.[21] The Bragg scattering averages over many unit cells. In this case, the extent of atomic displacements from ideal lattice sites is contained in the diffuse background, which is generally difficult to quantitatively obtain and analyze. The fact that solid solutions follow Vegard's law does not exclude them from having a bimodal distribution of the nearest-neighbor bond length, particularly when cations of the parents have different ionic radii. EXAFS is well-suited for the determination of near-neighbor spacing, especially relative to a well-defined standard such as the parents' compounds. It provides a direct and reliable characterization of the local structure, including distortions, present in solid solutions.

Local structural environment studies of other types of solid solutions (U monochalcogenides, zinc blend alloys) using EXAFS have revealed a complex local variation in the first- and second-neighbor distances[22–24] with bimodal distribution throughout the solid-solution composition and a deviation from Vegard behavior.

In the present study, the local structure around Th, U, and Pu in $Th_{1-x}M_xO_2$ solid solutions with M = U, Pu was determined by means of EXAFS spectroscopy over the entire range $x = 0$ to 1. The lattice parameters and interatomic distances of the cubic ThO_2-UO_2 and ThO_2-PuO_2 solid solutions are determined from XRD and EXAFS. The variation of the first- and second-shell bond length with dopant concentration is discussed for both mixed dioxides $Th_{1-x}U_xO_2$ and $Th_{1-x}Pu_xO_2$ and compared with XRD experiments.

Experimental Section

Sample Preparation. The oxalate route was chosen for synthesizing well-crystallized powdered samples with high homogeneity.[25]

$Th_{1-x}U_xO_2$ Samples. $Th_{1-x}U_xO_2$ mixed dioxides were prepared by mixing appropriate concentrated solutions of thorium chloride and uranium chloride in order to keep uranium in the tetravalent state. Tetravalent actinides were then coprecipitated with an excess of oxalic acid solution following the procedure already described.[26] Special attention was taken with regard to oxygen. The powder was calcined in a PYROX furnace at 1300 °C under a reducing atmosphere (Ar–4% H_2).

A series of thorium–uranium dioxides were prepared from the appropriate amounts of thorium and uranium chloride solutions, with mole ratios equal to 0.11, 0.24, 0.37, 0.49, 0.53, 0.67, 0.79, 0.81, and 0.91. The concentration of uranium and thorium incorporated in the solid was measured using PIXE analysis (particle-induced X-ray emission) and electron probe microanalysis (EPMA). The results obtained from both techniques were in good agreement with theoretical values. Moreover, microanalysis by electronic probe was used for testing the homogeneity of the stoichiometry of the samples. The values were determined with an uncertainty of ±0.01. In addition, X-ray photoelectron spectroscopy (XPS) was used for probing the chemical state of uranium at the surface. The fit of the $U_{4f(5/2)}$ and $U_{4f(7/2)}$ peaks correspond to the photoemission of U(IV) centered at 391 and 380.2 eV, typical of the binding energies of UO_2.

$Th_{1-x}Pu_xO_2$ Samples. Thorium nitrate solutions and plutonium nitrate in nitric solutions were mixed in stoichiometric conditions in order to get molar ratios equal to 0.12, 0.20, 0.32, and 0.66. Tetravalent actinides were coprecipitated by adding an excess of ammonium oxalate in nitric acid media ($C_2O_4^{2-}$ (0.2 M)/HNO_3 (3.5 M)). The precipitate was washed with deionized water, filtered, and finally dried. The mixed oxalates were calcined in a quartz tube at 900 °C for 12 h under air in a glovebox after they were preheated at 100 °C for 1 h.

The stoichiometry of the samples was obtained by measuring the concentration of both actinides using ICP-MS after complete dissolution in HNO_3 (14 M)/HF (5×10^{-2} M). The final

(14) Dawson, J. K. *J. Chem. Soc.* **1952**, 1882−1885.
(15) Mulford, R. N. R.; Ellinger, F. H. *J. Phys. Chem.* **1958**, *62*, 1466−1467.
(16) Martins, J. L.; Zunger, A. *Phys. Rev. B* **1984**, *30*, 6217−6220.
(17) Ridgway, M. C.; Yu, K. M.; Glover, C. J.; Foran, G. J.; Clerc, C. *Phys. Rev. B* **1999**, *60*, 10381−10386.
(18) Rothe, J.; Denecke, M. A.; Neck, V.; Muller, R.; Kim, J. I. *Inorg. Chem.* **2002**, *41*, 248−258.
(19) Barrett, N. T.; Greaves, G. N.; Willis, M. B. T.; Antonini, G. M.; Thornley, F. R. *J. Phys. C: Solid State Phys.* **1988**, *21*, L791−L796.
(20) Conradson, S. D.; Begg, B. D.; Clark, D L.; den Auwer, C.; Ding, M.; Dorhout, P. K.; Espinosa-Faller, F. J.; Gordon, P L.; Haire, R. G.; Hess, N. J.; Keogh, D. W.; Morales, L. A.; Neu, M. P.; Paviet-Hartmann, P.; Runde, W.; Drew Tait, C.; Veirs, D. K.; Villella, P. M. *J. Am. Chem. Soc.* **2004**, *126*, 13443−13458.
(21) Martin, P.; Ripert, M.; Petit, T.; Reich, T.; Hennig, C.; D'Acapito, F.; Hazemann, J. L.; Proux, O. *J. Nucl. Mat.* **2003**, *312*, 103−110.

(22) Mikkelson, J. C., Jr.; Boyce, J. B. *Phys. Rev. Lett.* **1982**, *49*, 1412−1415.
(23) Thorpe, M. F.; Garboczi, E. J. *Phys. Rev. B* **1990**, *42*, 8405−8417.
(24) Bombardi, A.; d'Acapito, F.; Mattenberger, K.; Vogt, O.; Lander, G. H. *Phys. Rev. B* **2003**, *68*, 10414−10417.
(25) Hubert, S.; Barthelet, K.; Fourest, B.; Lagarde, G.; Dacheux, N.; Baglan, N. *J. Nucl. Mat.* **2001**, *297*, 206−213.
(26) Heisbourg, G.; Hubert, S.; Dacheux, N.; Ritt, J. *J. Nucl. Mat.* **2003**, *321*, 141−151.

Table 1. Isotopic Composition of Pu

isotope	$t_{1/2}$ (years)	%
[239]Pu	24 110	97.09
[240]Pu	6563	2.87
[241]Pu	14.35	0.03
[242]Pu	375 000	0.0084
[238]Pu	87.7	0.0018

Table 2. Lattice Parameters and the First Two Shell Distances for Th$_{1-x}$U$_x$O$_2$ and Th$_{1-x}$Pu$_x$O$_2$[a]

composition (at %)	lattice parameter (Å)	average metal−oxygen distance (Å)	average metal−metal distance (Å)
	U		
0	5.598	2.424	3.958
11	5.585	2.418	3.949
24	5.574	2.414	3.941
37	5.545	2.401	3.920
49	5.550	2.403	3.924
52	5.531	2.395	3.911
67	5.519	2.390	3.902
79	5.507	2.384	3.893
81	5.490	2.377	3.882
91	5.477	2.371	3.872
100	5.471	2.369	3.869
	Pu		
0	5.5992	2.424	3.959
13	5.5858	2.419	3.950
20	5.5583	2.407	3.930
32	5.5401	2.399	3.917
66	5.4461	2.358	3.851
100	5.3936	2.335	3.814

[a] Standard error deviation for Th$_{1-x}$U$_x$O$_2$ solid solution is ±0.009; for Th$_{1-x}$Pu$_x$O$_2$ solid solution, ±0.0015 for $x \leq 0.20$ and ±0.0035 for $x \geq 0.32$.

Figure 1. Variation of the unit cell parameters with mole ratio x for Th$_{1-x}$U$_x$O$_2$.

Figure 2. Variation of the unit cell parameters with mole ratio x for Th$_{1-x}$Pu$_x$O$_2$.

compositions of the solid solutions correspond to $x = 0.13, 0.20, 0.32$, and 0.66. The values were determined with an uncertainty of ±0.035. Pure oxides ThO$_2$ and PuO$_2$ were also synthesized from the oxalate routes.
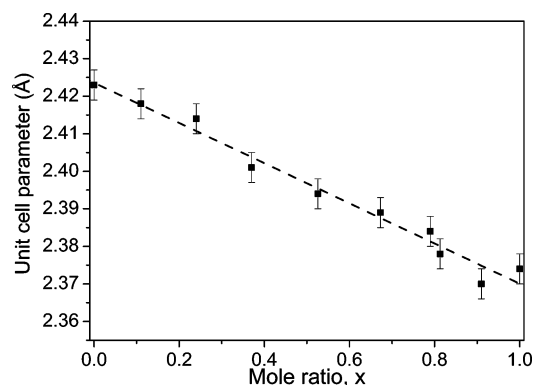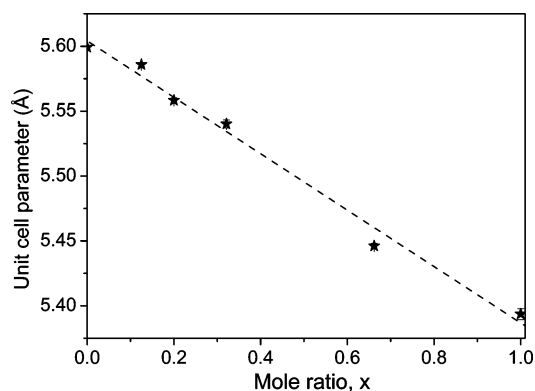
The isotopic composition of the plutonium used in the synthesis is described in Table 1. In this composition, the main isotope [239]Pu, which has a longer lifetime ($t_{1/2} = 24\ 110$ years) compared to [238]Pu ($t_{1/2} = 87.7$ years) and [241]Pu ($t_{1/2} = 14.35$ years) minimizes the creation of defects in the solid attributable to radiolysis effects.

XRD Characterization

All the samples were characterized using X-ray powder diffraction as described below.

Th$_{1-x}$U$_x$O$_2$ Characterization. X-ray powder diffraction data for all samples were obtained using a Philips PW 1050/70 diffractometer, using Cu Kα$_1$ ($\lambda = 1.5406$ Å) radiation. Silicon metal was added to the powder as an internal standard to calibrate the angular positions of the diffraction lines observed. The X-ray diffraction pattern of the mixed-oxide powders of various compositions is typical of the fluoride fcc structure. The lattice parameters of pure oxides ThO$_2$ and UO$_2$ were measured as $a = 5.598 \pm 0.009$ Å and $a = 5.471 \pm 0.012$ Å, respectively. They are in good agreement with the values reported by Lambertson et al.[11] and Cohen et al.[4] The average lattice parameters, calculated for all the compositions with the U-fit program,[27] are listed in Table 2, along with the average distances of the first ($R_{Th-O} = a\sqrt{3}/4$) and second coordination shells ($R_{Th-U} = a\sqrt{2}/2$).

(27) Evain, M.; *U−FIT: A Cell Parameter Refinement Program*; LMN: Nantes, France, 1992.

As expected, the lattice parameter decreases continuously as substitution of thorium ($r_{Th} = 1.05$ Å) by smaller, tetravalent uranium ($r_U = 0.997$ Å) increases. The presence of uranium in a higher oxidation state, which could not be observed in the XRD pattern, would tend to decrease the lattice parameter of the unit cell.[11] Figure 1 shows the variation of the mean lattice parameters with composition. The values obtained in this work for all compositions are in good agreement with that reported by Cohen et al.[4] for Th$_{1-x}$U$_x$O$_{2.0}$. A linear variation is observed throughout the entire solid solution, within the accuracy of the measurement, following Vegard's law. This confirms the formation of solid solutions.

Th$_{1-x}$Pu$_x$O$_2$ Characterization. X-ray powder diffraction data for all Th$_{1-x}$Pu$_x$O$_2$ samples were obtained with an INEL CPS 120 diffractometer (curved position-sensitive detector) using Cu Kα$_1$ radiation isolated by a germanium monochromator. Gold metal was added to the powder as an internal standard, in an epoxy resin, to calibrate the angular positions of the diffraction lines observed. The lattice parameters of pure dioxides ThO$_2$ and PuO$_2$ were measured as $a = 5.5992 \pm 0.0015$ Å and $a = 5.3936 \pm 0.0035$ Å, respectively. These values are in good agreement with the values reported in JCPDS 42-1462 and JCPDS 41-1170.

The average lattice constants calculated with the U-fit program[27] from the X-ray diffractogram are given in Table 2. The mean distances of the two first coordination shells calculated from the lattice constants are also listed. Figure 2 shows the variation of the mean lattice parameters with composition. As can be seen, the mean lattice constant decreases linearly with increasing mole ratio throughout the entire solid solution. This is consistent with a decrease in the cell parameter, which occurs on substitution of the large Th^{4+} by the small Pu^{4+}. The lattice parameters are in good

agreement with those calculated assuming Vegard's law, shown as the dashed straight line in Figure 2.

Local Atomic Structure Characterization by EXAFS

Sample Preparation. Among the $Th_{1-x}U_xO_2$ solid solutions prepared for the XRD characterization, six samples were used for EXAFS characterization, with $x = 0.11, 0.24, 0.49, 0.67, 0.79,$ and 0.91. All $Th_{1-x}Pu_xO_2$ samples ($x = 0.12, 0.20, 0.32,$ and 0.66), as well as the pure actinide dioxides ThO_2, UO_2, and PuO_2 ($x = 1$), already characterized by XRD, were also investigated by EXAFS.

The powders were finely ground and mechanically mixed with cellulose powder. The pellets were prepared by mixing $15-35$ mg/cm^2 powder, depending on the composition of the solid solutions, with 100 mg/cm^2 cellulose. The sample thickness was adjusted to attain absorption jumps ranging from 0.2 to 0.8, depending on the composition of the solid solutions. The samples were encapsulated in Kapton tape, mounted on an aluminum frame containing 3 samples, and placed inside a steel stainless chamber equipped with polycarbonate X-ray windows.

EXAFS Data Acquisition and Analysis. EXAFS measurements were performed at the "hot" beam line D44 (XAS4) of the LURE DCI synchrotron radiation facility, Orsay, France. The storage ring DCI operated at the average energy 1.85 GeV and a maximum stored current of 300 mA. A standard transmission scheme with a Ge (400) double crystal monochromator and two ion chambers containing argon gas were used. A vertical slit width of 0.5 mm situated ahead of the monochromator was used. The spectra were energy-calibrated by measurement of the transition spectrum of a Zr foil, where the energy of the first inflection point for the reference sample absorption edge was defined as 17 166.0 eV. Moreover, the Th (idem U and Pu) spectra were self-calibrated; at the beginning of the analysis, the Th edges of all spectra were aligned to within 0.3 eV from the first inflection point in the XANES.

X-ray absorption spectra were measured in the energy interval $16\,200-17\,120$ eV for the Th L_{III} edge, $17\,050-18\,050$ eV for the U L_{III} edge, and $18\,000-19\,000$ eV for the Pu L_{III} edge, using steps of 2 eV in a transmission mode for all the investigated samples. Several acquisitions ($4-10$ spectra, depending on the composition) were carried out on the same sample to improve the signal-to-noise ratio. Each EXAFS spectrum was extracted and fitted individually. For the same composition, the obtained structural parameters were averaged.

EXAFS spectra were treated using the EDA (EXAFS Data Analysis) software package following the standard procedure.[28] The E_0 position, defining the zero wave vector ($k = 0$), was set at the energies 16 300 eV for Th, 17 169 eV for U, and 18 056 eV for Pu. Particular attention was devoted to the EXAFS zero-line removal (background and multielectron contributions) through a multistep polynomial/cubic spline procedure in order to have a correct behavior of the EXAFS signal from small wave vector values. The experimental EXAFS spectra $\chi(k)k^2$ obtained at the Th and U(Pu) L_{III} edges were Fourier transformed (FT) in the $0.0-15.0$ $Å^{-1}$ range using a Kaiser−Bessel window function. In all the FTs of the experimental spectra, two main peaks at 1.9 and 3.8 Å were observed. The EXAFS signals from the first two peaks were singled out using the back-Fourier filtering within the ranges $1.1-2.6$ and $2.8-4.6$ Å, respectively, and fitted within the reduced k-space ranges $2-12$ and $4-14$ $Å^{-1}$, respectively.

To achieve composition dependence of the structural parameters with high accuracy, we obtained the backscattering phases $\phi(\pi,k)$

and amplitudes functions $f(\pi,k)$ experimentally from the pure dioxides (semiempirical method). Additionally, the backscattering phases $\phi(\pi,k)$ and amplitude functions $f(\pi,k)$ were calculated by theoretical FEFF8 code[29,30] to obtain absolute values of the Debye-Waller factors (DW).

Theoretical $\phi(\pi,k)$ and $f(\pi,k)$ values were calculated using different clusters selected to mimic the possible environment of the M^{4+} ions in the solid solutions. A self-consisted potential with a complex Hedin−Lundqvist exchange−correlation part was used. Calculations were performed within an ab initio multiple scattering (MS) model[29] for high-symmetry clusters [MO_8, $M_{12}O_{24}$, M_6O_{24}] with M = Th, U, and Pu with known crystallographic data for ThO_2, UO_2, and PuO_2. We carried out the calculations with a cluster of 65 atoms within the 6 Å radius, taking into account all single scattering (SS) paths (5) and MS paths (9) up to the third order and up to 6 Å.

In the semiempirical approach, the analysis of the composition-dependent EXAFS signals was performed using a best-fit procedure within the single-scattering harmonic approximation with the experimental amplitude and phase-shift functions, taken from the pure dioxide EXAFS signals at room temperature. The relative values of the distances (R) and DW factors were treated as free parameters, whereas the coordination numbers were constrained at crystallographic values. Because the E_0 value is not composition-dependent, it was set to the same value at all compositions.

For the solid solutions, we constrain the parameters to get integer values of coordination number $N = 8$ for the first-shell and $N = 12$ for the second-shell EXAFS contributions with similar back-scattering functions of the Th−Th, Th−U, U−Th, and U−U pairs. As far as we are interested in the relative changes in the distance with composition, we have made the assumption that the third cumulant is close to zero, which seems reasonable in light of the relatively low thermal expansion coefficient of the mixed actinide.

The statistical uncertainty of the fitting procedure is represented by error bars in the figures. Systematic errors of individual files can be estimated by the scattering of the values with respect to smooth composition dependence.

Experimental $f(\pi,k)$ and $\phi(\pi,k)$ for the first and second shells were extracted from the experimental EXAFS data obtained on crystalline ThO_2, UO_2, and PuO_2. These functions were obtained from the fit with the theoretical phase and amplitude, assuming a Gaussian distribution with $N = 8$ and $R = 2.4238$ Å (Th−O), $R = 2.3688$ Å (U−O), and R = 2.336 Å (Pu−O) from the crystallographic data, and $\sigma^2 = 0.005$ $Å^2$. Note that the use of experimental phases and amplitudes to a certain extent allows for the compensation of systematic errors, including the contribution of the mean free path, the multielectron amplitude reduction factor S^2_0, glitches, and resolution, which reduces the number of adjustable parameters and consequently increases the reliability of the fit results. To ensure transferability of phase and amplitude and to allow estimation of systematic errors, we analyzed all the data in a similar way, using the same experimental phases and amplitudes, filtering procedures, and parameters.

$Th_{1-x}U_xO_2$ Solid Solutions. We have analyzed the Th and U L_{III} edge EXAFS of eight samples to determine the change in the Th−O, Th−U(Th) and U−O, U−Th(U) bond lengths, R_{Th-O}, R_{Th-U} and R_{U-O}, R_{U-Th}, as a function of solid-solution composition. The k^2-weighted EXAFS spectra and their FTs obtained for three different compositions of $Th_{1-x}U_xO_2$ are shown in Figures 3 and
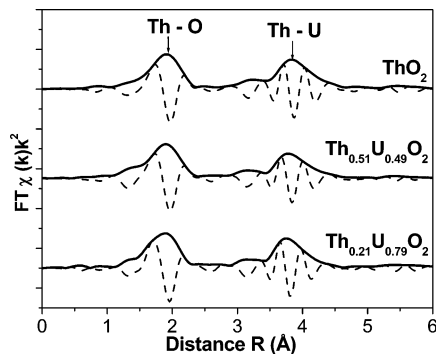
(28) Kuzmin, A. *Physica B* **1995**, *208/209*, 175−176. Kuzmin, A. *J. Phys. IV* **1997**, *7*, C2-213−C2-214.

(29) Rehr, J. J.; Mustre de Leon, J.; Zabinsky, S. I.; Albers, R. C. *J. Am. Chem. Soc.* **1991**, *113*, 5135−5140.
(30) Mustre de Leon, J.; Rehr, J. J.; Zabinsky, S. I.; Albers, R. C. *Phys. Rev. B* **1991**, *44*, 4146−4156.
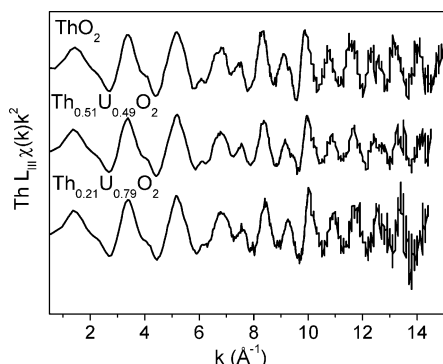
Figure 3. Experimental $\chi(k)k^2$ EXAFS spectra at the Th L$_{III}$ edge for ThO$_2$, Th$_{0.61}$U$_{0.48}$O$_2$, and Th$_{0.21}$U$_{0.78}$O$_2$.

Figure 5. Experimental $\chi(k)k^2$ EXAFS spectra at the Pu L$_{III}$ edge for Th$_{0.87}$Pu$_{O.13}$O$_2$, Th$_{0.68}$Pu$_{0.32}$O$_2$, and Th$_{0.34}$Ru$_{0.66}$O$_5$.

Figure 4. Fourier transforms (FT) to real space measured at the Th L$_{III}$ edge for ThO$_2$, Th$_{0.51}$U$_{0.49}$O$_2$, and Th$_{0.21}$U$_{0.79}$O$_2$. Modulus and imaginary parts of the FTs were not corrected for the photoelectron phase shift; therefore, the positions of the peaks differ up to 0.5 Å from the true crystallographic values.

Figure 6. Fourier transforms (FT) to real space measured at the Pu L$_{III}$ edge for PuO$_2$, Th$_{0.34}$Pu$_{0.66}$O$_2$, and Th$_{0.68}$Pu$_{0.32}$O$_2$. Modulus and imaginary parts of the FTs were not corrected for the photoelectron phase shift; therefore, the positions of the peaks differ up to 0.5 Å from the true crystallographic values.

4, respectively, for the Th L$_{III}$ edge. In all the FTs, the same features are observed: two main peaks located at 1.9 and 3.8 Å, a smaller pre-peak at 3.2 Å, and weaker peaks from 4.5 to 6 Å. The EXAFS signals from the first two peaks were singled out by Fourier filtering. The first peak in the range 1.1−2.6 Å is related to the first coordination sphere (Th−O bond), which is composed of eight oxygen atoms. The second peak and pre-peak, ranging between 2.8 and 4.6 Å, are mainly due to 12 metal atoms of the second coordination sphere, which consists of either thorium atoms or thorium and uranium atoms, depending on the composition of the solid solution. However, there is an additional contribution due to 24 oxygen atoms located in the third coordination sphere and MS contributions.
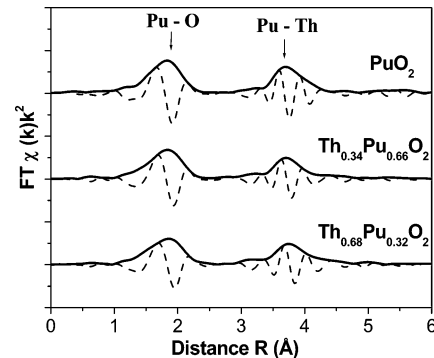
These contributions are generally weak but not negligible and appear as a small shoulder at the right-hand side of the second peak (Figure 4). The peaks beyond the second one are due to the more distant shells composed of thorium, uranium, and oxygen atoms. Their EXAFS signals do not overlap in R-space. They are slightly influenced by the MS effects because of a small number of linear atom chains in the structure. As a result, the analysis of this region is not part of this paper.

Generally, the first peak in the Th and U L$_{III}$ edge FT of the solid solutions is sharp and shows a small shift (see imaginary part) from a larger distance (ThO$_2$) toward UO$_2$. This behavior is due to gradual variation in the first coordination shell M−O distance with composition. The second peak is also sharp and displays more visible gradual shift (see imaginary part) toward the end member distance, as the second shell is composed of mixed atoms. The absence of any significant contribution near $R = 0$ Å indicates a good removal of background absorption μ_0.

Th$_{1-x}$Pu$_x$O$_2$ Solid Solutions. The EXAFS spectra were treated following the same procedure used for Th$_{1-x}$U$_x$O$_2$ described above. We have analyzed the Th and Pu L$_{III}$ edge EXAFS of three solid solutions to determine the change in the Th−O, Th−Pu(Th) and Pu−O, Pu−Th(Pu) bond lengths, R_{Th-O}, R_{Th-Pu} and R_{Pu-O}, R_{Pu-Th}, as a function of solid-solution composition. The k^2-weighted $\chi(k)$ spectra obtained for the three compositions of Th$_{1-x}$Pu$_x$O$_2$ at the Th and Pu L$_{III}$ edge are presented in Figure 5. Their FTs are shown Figure 6. They exhibit the same features as those for Th$_{1-x}$U$_x$O$_2$: two main peaks located at 1.9 and 3.8 Å, a smaller pre-peak at 3.2 Å, and weaker peaks from 4.5 to 6 Å.

Results and Discussion

The interpretation of the EXAFS in pure ThO$_2$, UO$_2$, and PuO$_2$ has been done using the MS approach.[19,31−33] It was found that the features observed in the experiment are due to scattering within about a five-shell cluster of 6.0 Å radius. An early interpretation of the EXAFS spectra of the UO$_2$ crystal at room temperature[19] reports a U−O distance of 2.43 Å, which is greater than the crystallographic distance of 2.368 Å by 0.062 Å. This was attributed to the anharmonicity in the lattice vibrations (distortion of the local environment around uranium ions). The reported U−U distance of 3.89 Å closely matches with the crystallographic distance of 3.87 Å.

(31) Wu, Z.; Farges, F. *Physica B* **1999**, *266*, 282−289.
(32) Kalkowski, G.; Kaindl, G.; Brewer, W. D.; Krone, W. *Phys. Rev. B* **1986**, *35*, 2667−2677.
(33) Begg, B. D.; Hess, N. J.; Weber, W. J.; Conradson, S. D.; Schweiger, M. J.; Ewing, R. C. *J. Nucl. Mat*. **2000**, *278*, 212−224.

Table 3. $Th_{1-x}U_xO_2$ Fit Results for the First Two Coordination Shells at the Th and U L_{III} edges

| solid	first shell			second shell		
	R_{Th-O} (Å)	R_{U-O} (Å)	$\langle R_{Me-O}\rangle^a$	R_{Th-An} (Å)	R_{U-An} (Å)	$\langle R_{Me-Me}\rangle^a$
ThO_2	2.424^b		2.424^b	3.959^b		3.959^b
$Th_{0.89}U_{0.11}O_2$	2.423	2.395	2.419	3.950	3.940	3.949
$Th_{0.76}U_{0.24}O_2$	2.418	2.386	2.411	3.939	3.926	3.936
$Th_{0.51}U_{0.49}O_2$	2.417	2.378	2.398	3.923	3.906	3.915
$Th_{0.33}U_{0.67}O_2$	2.412	2.376	2.388	3.917	3.895	3.903
$Th_{0.21}U_{0.79}O_2$	2.404	2.373	2.380	3.901	3.884	3.887
$Th_{0.09}U_{0.91}O_2$	2.406	2.372	2.376	3.900	3.878	3.880
UO_2		2.369^b	2.369		3.865^b	3.865^b

^{a} $\langle R_{Me-O(Me)}\rangle$: calculated composition weighted average distance. ^{b} Calculated from XRD data[11,4] for ThO_2 and UO_2, respectively.

Table 4. $Th_{1-x}Pu_xO_2$ Fit Results for the First Two Coordination Shells at the Th and Pu L_{III} edges

solid	first shell			second shell		
	R_{Th-O} (Å)	R_{Pu-O} (Å)	$\langle R_{Me-O}\rangle^a$	R_{Th-An} (Å)	R_{Pu-An} (Å)	$\langle R_{Me-Me}\rangle^a$
ThO_2	2.424^b		2.424^b	3.959^b		3.959^b
$Th_{0.87}Pu_{0.13}O_2$	2.422	2.373	2.415	3.952	3.901	3.945
$Th_{0.68}Pu_{0.32}O_2$	2.416	2.367	2.400	3.935	3.890	3.921
$Th_{0.34}Pu_{0.66}O_2$	2.407	2.352	2.370	3.889	3.843	3.858
PuO_2		2.336^b	2.336^b		3.814^b	3.814^b

^{a} $\langle R_{Me-O(Me)}\rangle$: calculated composition weighted average distance. ^{b} Calculated from XRD data[11,20] for ThO_2 and PuO_2, respectively.

The interpretation of EXAFS in the studied solid solutions is analogous to pure oxides because of the very small differences in the scattering amplitude and phase-shift functions of thorium and uranium (plutonium) atoms. The visible differences in the EXAFS with solid-solution composition can be caused only by the change in the lattice constant as the scattering amplitude and phase-shift functions between thorium and uranium (plutonium) atoms are very small.

First-Shell Environment. The first-shell distances obtained from fits to the experimental data at the Th, U, and Pu L_{III} edges, for all compositions of both solid solutions $Th_{1-x}U_xO_2$ and $Th_{1-x}Pu_xO_2$, are given in Tables 3 and 4. We estimate an uncertainty of 0.003 Å in the near-neighbor distances, as the point at which the reliability of fit parameters increases by a factor of 2 from a minimum value, except in the dilute compound (10 mol %), where the error is ~0.005 Å. This error bar is low as far as we compare different measurements using experimental amplitude and phase-shift functions.

The Th−O and U−O interatomic distances are plotted as a function of dopant concentration in Figure 7, in comparison with the calculated average distances from XRD and EXAFS measurements. The R_{U-O} and R_{Th-O} distances, which are shown by the lower and upper curves, vary slightly upon dilution in the solid solution. The same behavior is observed in Figure 8 for the first neighbor distances in $Th_{1-x}Pu_xO_2$.

The total decrease of R_{Th-O} in $Th_{1-x}U_xO_2$ from pure ThO_2 to pure UO_2 (linear interpolation to 0 mol % Th in UO_2) is 0.019 ± 0.003 Å, whereas the variation calculated from the lattice constants for ThO_2 and UO_2 is 0.055 Å. At the same time, the increase in R_{U-O} from pure UO_2 to the impurity limit of U in ThO_2 (linear interpolation to 0 mol % U in ThO_2) is 0.026 ± 0.003 Å. It is readily apparent that the R_{Th-O} and R_{U-O} values differ substantially from the weighted average cation−anion distance (VCA model), shown in the middle curve of Figure 7. However, the weighted mean
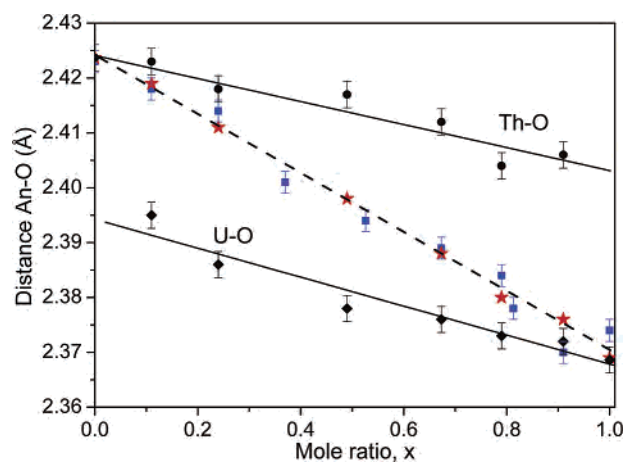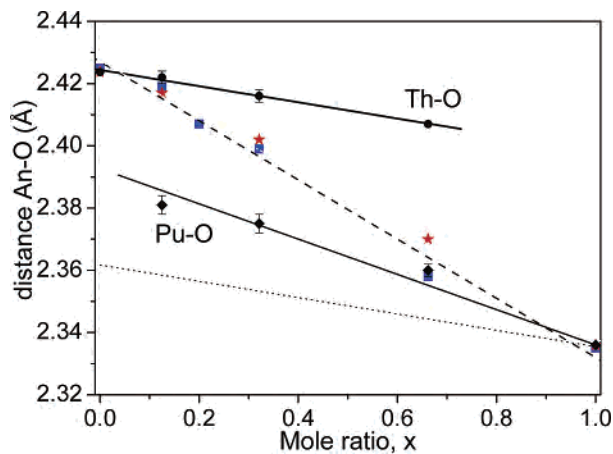

Figure 7. Interatomic distances Th−O (● upper line) and U−O (◆ bottom line) vs composition in $Th_{1-x}U_xO_2$ solid solutions. The solid lines represent a least-squares fit to the experimental values. Dashed line is the VCA metal−oxygen distance calculated from XRD (■) and EXAFS (★) measurements.

cation−anion NN distance calculated is equal to the virtual-crystal distance within the experimental error bar. The R_{Th-O} distance can be expressed as $R_{Th-O} = 2.424 - 0.019x$, whereas the R_{U-O} distance can be derived from the following equation: $R_{U-O} = 2.394 - 0.026x$. The composition dependence of R_{U-O} bond length is slightly larger than that of the R_{Th-O} bond length. This situation corresponds to a bimodal near-neighbor distribution. For low uranium concentration (below $x = 0.2$), a small departure from the linear dependence of R_{U-O} can be observed; however, more experimental data are needed in this concentration range to confirm this tendency. Nevertheless, the composition weighted average of the two distances is very close to the average one obtained from XRD, as shown in the middle curve of Figure 7.

Another observation is that the DW factor (σ^2) of the first-shell distribution of Th−O and U−O is essentially the same as that in ThO_2 or UO_2 within 0.001 Å^2, i.e., we measure no

Figure 8. Interatomic distances Th−O (● upper line) and Pu−O (◆ bottom line) vs composition in Th$_{1-x}$U$_x$O$_2$ solid solutions. The solid lines represent a least-squares fit to the experimental values. Dashed line is the expected Vegard distance calculated from XRD (■) and EXAFS data. (★). Dotted line represents parallel line to the composition dependence of Th−O.

additional broadening, either from dynamic or static contributions. The DW factor for the whole range of solid solutions within the error of the experiments did not change and was equal to $\sigma^2 = 0.005 \pm 0.001$ Å^2 in the Th−O and U−O near-neighbor distributions. We conclude that it is mainly determined by thermal vibrations, but the local deformations connected with the difference of the ionic radii of thorium and uranium give a comparatively small contribution to the total DW factor. Additional EXAFS measurements at low temperature will be useful for studying this effect.

Figure 8 shows experimental values of $R_{Th−O}$ and $R_{Pu−O}$ (upper and lower curves) as a function of composition. As for Th$_{1-x}$U$_x$O$_2$, two distinct values are obtained for both $R_{Th−O}$ and $R_{Pu−O}$ distances, which confirm the bimodal distribution of the first-coordination-shell distance. A linear decrease in the An−O distances is observed with the increase in Pu content. The total decrease in $R_{Th−O}$ from pure ThO$_2$ to pure PuO$_2$ (linear interpolation to 0 mol % Th in PuO$_2$) is 0.025 $\pm$ 0.003 Å, whereas the variation calculated from the lattice constants for ThO$_2$ and PuO$_2$ is 0.089 Å. The composition dependence of $R_{Th−O}$ is similar to that obtained in Th$_{1-x}$U$_x$O$_2$, although the radii difference between parents is larger in Th$_{1-x}$Pu$_x$O$_2$. However, the composition dependence of $R_{Pu−O}$ from pure PuO$_2$ to ThO$_2$ (linear interpolation to 0 mol % Th in PuO$_2$) is about twice as large, i.e, 0.055 $\pm$ 0.005 Å. The $R_{Th−O}$ distance can be expressed as $R_{Th\ O} = 2.424 - 0.025x$, whereas the $R_{Pu−O}$ distance can be derived from the following equation: $R_{Pu−O} = 2.391 - 0.055x$. Although the number of samples is smaller than for Th$_{1-x}$U$_x$O$_2$, the greater slope of the linear variation $R_{(M−O)} = f(x)$, observed for the smallest cation in Th$_{1-x}$Pu$_x$O$_2$, is confirmed. This means that the smaller cation (U, Pu) exhibits a larger deviation from ideal Vegard predicted behavior. Whereas Th−O distances are similar in both Th$_{1-x}$U$_x$O$_2$ and Th$_{1-x}$Pu$_x$O$_2$ solid solutions, the dopant−oxygen bond compensates by expanding their bond as much as their concentration decreases and the radii difference between the end compounds increases. Similar to that in the former solid solution, the weighted composition

mean distances obtained from EXAFS are close from the ones measured from XRD.

Second-Shell Environment. There are various ways in which the three-dimensional lattice can distort to accommodate two different cation−anion distances. Moredistant information can suggest the nature of this distortion. Mikkelsen and Boyce, analyzing the EXAFS of Ga$_{1-x}$In$_x$As alloys,[22,34] have previously suggested that the uncertainty in the more-distant EXAFS analysis increases for several reasons. First, the contribution to the EXAFS decreases rapidly with distance from the central atom, decreasing the signal-to-noise-ratio. Second, the more-distant FT peaks are less separated, which means a possible interference between peaks. Third, in solid-solutions, there will be greater interference between backscattering waves from atoms of different kinds (or at different distances) in the same shell, reducing the sensitivity of the models. Finally, the fits will include at least two Gaussians, with six or more adjustable parameters. Fortunately, the EXAFS spectra of actinide dioxide solid solutions are very favorable for the analysis (high backscattering amplitudes and small DW factors as well as similar phases for Th−Th, Th−U, U−Th, and U−U pairs) and good fits were obtained with physically realistic parameters using the analysis procedure described above.

First, the contribution at 3.8 Å of second neighbors to the EXAFS is evident from the data in Figures 3−5. Second, the second-neighbor FT peak is well separated, which means there is small interference between the peaks. Third, in solid-solutions Th$_{1-x}$U$_x$O$_2$ and Th$_{1-x}$Pu$_x$O$_2$, the interference between backscattered waves from atoms of different kinds (Th, U, Pu) in the second shell is constructive because of practically identical backscattering amplitudes and phases. Therefore, fits include only one Gaussian or asymmetric Gaussian, with three or four adjustable parameters.

The second-shell distances obtained from the fits to the EXAFS at the Th, U, and Pu L$_{III}$ edges, for all compositions of Th$_{1-x}$U$_x$O$_2$ and Th$_{1-x}$Pu$_x$O$_2$ solid solutions, are given in Tables 3 and 4. The resulting distances $R_{Th−U(Th)}$, $R_{U−Th(U)}$ and $R_{Th−Pu(Th)}$, $R_{Pu−Th(Pu)}$ are plotted versus composition in Figures 9 and 10 for Th$_{1-x}$U$_x$O$_2$ and Th$_{1-x}$Pu$_x$O$_2$, respectively, in comparison with the mean distances calculated from XRD and EXAFS measurements. Contrary to the first shell, the U−U(Th) and Th−Th(U) distances vary strongly with composition (Figure 9). The total decrease in $R_{Th−Th(U)}$ from pure ThO$_2$ to pure UO$_2$ (linear interpolation to 0 mol % Th in UO$_2$) is 0.065 $\pm$ 0.003 Å, whereas the difference calculated from the lattice constant for ThO$_2$ and UO$_2$ is 0.094 Å. At the same time, the increase in $R_{U−Th(U)}$ from pure UO$_2$ to pure ThO$_2$ (linear interpolation to 0 mol % U in ThO$_2$) is 0.083 $\pm$ 0.003 Å. Moreover, the weighted mean of these various distances is very close to the VCA average distance, as shown in Figure 9. These experimental cation−cation distance measurements point out that on the atomic scale, appreciable clustering is absent in Th$_{1-x}$U$_x$O$_2$.

In the case of Th$_{1-x}$Pu$_x$O$_2$, the same behavior is observed from the analysis of cation−cation distances $R_{Th−Pu(Th)}$ and

(34) Mikkelson, J. C., Jr.; Boyce, J. B. *Phys. Rev B* **1983**, *28*, 7130−7140.
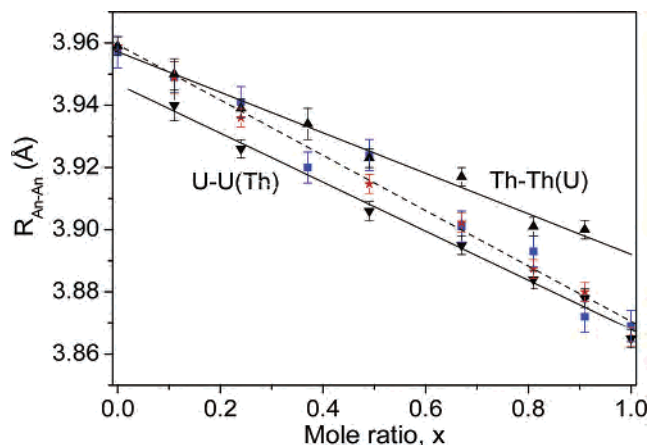
Figure 9. Variation of interatomic distances Th−U(Th) (▲ upper line) and U−Th(U) (▼ bottom line) with composition. Middle curve is the VCA cation−cation distance calculated from XRD (■) and EXAFS (★) data.
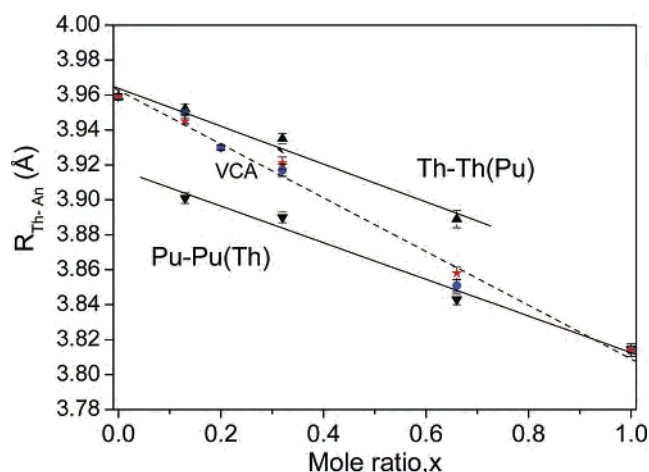
Figure 10. Variation of interatomic distances Th−Th(Pu) (▲ upper line) and Pu−Pu(Th) (▼ bottom line) with composition. Middle curve is the VCA cation−cation distance calculated from XRD (●) and EXAFS (★) data.

$R_{Pu-Th(Pu)}$. The total decrease in $R_{Th-Th(Pu)}$ from pure ThO_2 to pure PuO_2 (linear interpolation to 0 mol % Th in PuO_2) is 0.104 ± 0.010 Å, whereas the difference calculated from the lattice constant for ThO_2 and PuO_2 is 0.145 Å. At the same time, the increase in $R_{Pu-Pu(Th)}$ from pure PuO_2 to pure ThO_2 is similar, at 0.103 ± 0.010 Å. The weighted mean of these various distances is very close to the VCA average distance, as shown in Figure 10. Therefore, as in the case of $Th_{1-x}U_xO_2$, the experimental cation−cation distance mea-

surements point out that on the atomic scale, appreciable clustering is absent in $Th_{1-x}Pu_xO_2$.

Conclusion

From EXAFS measurements at the Th, U, and Pu L_{III} edges of each composition of both $Th_{1-x}U_xO_2$ and $Th_{1-x}Pu_xO_2$ systems, the first- and second-shell distances were extracted with high accuracy. Compared to the values obtained from XRD measurements, the weighted mean cation−anion and cation−cation bond lengths determined from EXAFS data are very close. They vary linearly with composition, following Vegard's law.

However, in the first-shell spacing, interatomic distances R_{Th-O} and $R_{U(Pu)-O}$ are readily distinct and vary slightly with composition. The Th−O and U−O distances change by only 0.019 and 0.026 Å, respectively, whereas the average first-neighbor distance, calculated from the lattice constants for ThO_2 and UO_2, changes by 0.055 Å for x ranging from 0 to 1. In $Th_{1-x}Pu_xO_2$ solid solutions, the same behavior is emphasized, with a larger composition dependency of R_{Pu-O} compared to that of R_{Th-O}. The Th−O and Pu−O distances change by 0.025 and 0.0425 Å, respectively, whereas the average distance calculated from the lattice constants for ThO_2 and PuO_2 changes by 0.079 Å for x ranging from 0 to 1. The smallest cation−oxygen bond in solid solution tends to compensate by expanding the bond as much as the bond length difference between parents increases. By comparison, the mean first-shell distances change by 0.054 and 0.089 Å in $Th_{1-x}U_xO_2$ and $Th_{1-x}Pu_xO_2$, respectively.

The second-shell results obtained for both solid solutions $Th_{1-x}U_xO_2$ and $Th_{1-x}Pu_xO_2$ indicate that the cation−cation distances are closer to the VCA model and vary more strongly with composition. The Th−Th(U) and U−U(Th) distances change by 0.069 and 0.082 Å, compared to the calculated average distance of 0.094 Å. In $Th_{1-x}Pu_xO_2$ solid solutions, a greater variation with composition occurs: 0.104 and 0.103 Å for Th−Th(Pu) and Pu−Pu(Th), respectively, compared to 0.126 Å for the calculated average distance change. The experimental cation−cation distance measurements point out that on the atomic scale, appreciable clustering is absent in both solid solutions $Th_{1-x}U_xO_2$ and $Th_{1-x}Pu_xO_2$.